PLOS ONE

RESEARCH ARTICLE

Real-time carbon allocation into biogenic volatile organic compounds (BVOCs) and respiratory carbon dioxide (CO_2) traced by PTR-TOF-MS, $^{13}CO_2$ laser spectroscopy and ^{13}C-pyruvate labelling

Lukas Fasbender*, Ana Maria Yáñez-Serrano, Jürgen Kreuzwieser, David Dubbert, Christiane Werner

Ecosystem Physiology, Institute of Forest Sciences, Faculty of Environment and Natural Resources, Albert-Ludwigs-University Freiburg, Freiburg, Germany

* lukas.fasbender@cep.uni-freiburg.de

Citation: Fasbender L, Yáñez-Serrano AM, Kreuzwieser J, Dubbert D, Werner C (2018) Real-time carbon allocation into biogenic volatile organic compounds (BVOCs) and respiratory carbon dioxide (CO_2) traced by PTR-TOF-MS, $^{13}CO_2$ laser spectroscopy and ^{13}C-pyruvate labelling. PLoS ONE 13(9): e0204398. https://doi.org/10.1371/journal.pone.0204398

Editor: Riikka Rinnan, University of Copenhagen, DENMARK

Received: September 13, 2017

Accepted: September 7, 2018

Published: September 25, 2018

Data Availability Statement: All relevant data are within the paper and its Supporting Information files.

Funding: This work was supported by the European Research Council (ERC) Project VOCO2 (647008). The funders had no role in study design, data collection and analysis, decision to publish, or preparation of the manuscript.

Abstract

Our understanding of biogenic volatile organic compound (BVOC) emissions improved substantially during the last years. Nevertheless, there are still large uncertainties of processes controlling plant carbon investment into BVOCs, of some biosynthetic pathways and their linkage to CO_2 decarboxylation at central metabolic branching points. To shed more light on carbon partitioning during BVOC biosynthesis, we used an innovative approach combining $\delta^{13}CO_2$ laser spectroscopy, high-sensitivity proton-transfer-reaction time-of-flight mass spectrometry and a multiple branch enclosure system in combination with position-specific ^{13}C-metabolite labelling. Feeding experiments with position-specific ^{13}C-labelled pyruvate, a central metabolite of BVOC synthesis, enabled online detection of carbon partitioning into ^{13}C-BVOCs and respiratory $^{13}CO_2$. Measurements of trace gas emissions of the Mediterranean shrub *Halimium halimifolium* revealed a broad range of emitted BVOCs. In general, [2-13C]-PYR was rapidly incorporated into emitted acetic acid, methyl acetate, toluene, cresol, trimethylbenzene, ethylphenol, monoterpenes and sesquiterpenes, indicating *de novo* BVOC biosynthesis of these compounds. In contrast, [1-13C]-pyruvate labelling substantially increased $^{13}CO_2$ emissions in the light indicating C1-decarboxylation. Similar labelling patterns of methyl acetate and acetic acid suggested tightly connected biosynthetic pathways and, furthermore, there were hints of possible biosynthesis of benzenoids via the MEP-pathway. Overall, substantial CO_2 emission from metabolic branching points during *de novo* BVOC biosynthesis indicated that decarboxylation of [1-13C]-pyruvate, as a non-mitochondrial source of CO_2, seems to contribute considerably to daytime CO_2 release from leaves. Our approach, combining synchronised BVOC and CO_2 measurements in combination with position-specific labelling opens the door for real-time analysis tracing metabolic pathways and carbon turnover under different environmental conditions, which may enhance our understanding of regulatory mechanisms in plant carbon metabolism and BVOC biosynthesis.

Competing interests: The authors have declared that no competing interests exist.

Introduction

Our understanding on emissions of biogenic volatile organic compounds (BVOCs), including thousands of different compounds from different chemical classes, has improved substantially during the last decades, partially due to new developments in measuring techniques. Therefore, the biosynthetic pathways of a great number of volatile compounds such as isoprenoids, wound induced compounds or several oxygenated compounds (e.g. acetaldehyde, ethanol, methanol) are well—but still not fully—understood. In contrast, very little is known on the underlying biochemical production processes of many other volatiles (e.g. benzenoids, methyl acetate), the regulation of plant carbon investment into such BVOCs, as well as environmental factors controlling biosynthesis and emission of these compounds. Moreover, unknown processes and key determinants controlling BVOC release from terrestrial vegetation account for large uncertainties in our understanding of global carbon cycling [1,2]. Although ^{13}C-labelling experiments already improved our knowledge on carbon allocation into BVOCs [3–5], there are still open questions regarding carbon partitioning into plant primary and secondary (e.g. BVOC emissions) metabolism with special regard to the biochemical link between both.

Noteworthy, the complex biosynthetic pathways of many volatiles produced in plants are tightly linked to CO_2 exchange between the plant and the atmosphere. For example, biosynthesis of monoterpenes and isoprene, the latter being the most important volatile emitted by vegetation, takes place in the chloroplasts and uses Calvin cycle intermediates (pyruvate and glyceraldehyde-3-phosphate) as direct precursors. Hence, production of these compounds is tightly linked to photosynthetic CO_2 fixation [5,6]. On the other hand, use of the key metabolite pyruvate as a precursor often involves a decarboxylation step during biosynthesis, in which the carboxyl group of pyruvate is released as CO_2 [7–9]. Thus, many pathways producing BVOCs constitute a source of CO_2 even in the light, besides the main CO_2 releasing process in plants, mitochondrial dark respiration. Hence, there are at least four main processes determining the CO_2 exchange in plants, *i.e.* CO_2 fixation during photosynthesis, photorespiration, CO_2 generating processes in metabolic pathways and mitochondrial respiration mainly taking place in the tricarboxylic acid (TCA)-cycle. From an analytical point of view, mitochondrial respiration can easily be determined in the absence of light, however, it is at least partially inhibited in the light [7,10–14]. In contrast, analysing CO_2 evolving processes during the day is tricky due to co-occurring photosynthesis. Moreover, in the light multiple sources of CO_2 production exist, as during production of BVOCs whose link to CO_2 production has not been well established so far [15]. Tcherkez et al. (2017) point out that a comprehensive analysis of metabolic fluxes, including partitioning at branching points, is still lacking and that the specific origin of carbon atoms fuelling day-respiration is still uncertain.

To unravel metabolic networks, the use of central metabolites, which are position-specific labelled with stable isotopes, reflects a very effective tool in order to follow the metabolic fate of the tracer into different anabolic and catabolic pathways [15,16]. As mentioned above, pyruvate is a central metabolite tightly linking plant primary and secondary metabolism. In the present study, we therefore fed plants with position-specific labelled pyruvate (pyruvate ^{13}C-labelled at the C1 or C2-carbon position). This approach enables tracing the fate of single ^{13}C-atoms of pyruvate through metabolic branching points into volatile plant metabolites and CO_2 and allows to investigate their metabolic pathways.

Preliminary experiments indicated the vast potential of combining proton-transfer-reaction mass spectrometry (PTR-MS) with molecular tracer approaches for better understanding carbon partitioning in plants [17–20]. Because incorporation of tracers into individual volatiles happens at short temporal scales and dynamics are diverse for different compounds, quantification of these processes needs precise and synchronized analytical systems. Therefore, we

used highly sensitive proton transfer reaction time-of-flight mass spectrometry (PTR-TOF-MS) with stable isotope CO_2 infrared laser spectroscopy (IRIS) and combined this technological infrastructure with position-specific molecular labelling. We aimed at analyzing the trace gas emissions of a Mediterranean shrub *Halimium halimifolium* under standardized environmental conditions. On the one hand, Mediterranean shrubs from the *Cistaceae* family possess a very active secondary metabolism resulting in the biosynthesis of a plethora of plant secondary metabolites including many BVOC [21,22]. On the other hand, *H. halimifolium* exhibits large variations in day respired $\delta^{13}CO_2$ [8,23,24], suggesting a, so far speculative, link to plant secondary metabolism [15,16,25,26].

In particular, we aim to identify and quantify the range of BVOC emitted from *H. halimifolium* shoots, link BVOC emission with day released CO_2 and explore the underlying pathway. To this end, we take advantage of our system, which enables to trace the fate of ^{13}C derived from either [1-13C]-pyruvate (PYR) or [2-13C]-pyruvate into BVOCs and CO_2 in real-time. We anticipated that traceability of ^{13}C in different volatile compounds may help elucidating biosynthetic pathways particularly of less studied compounds that are still unclear or not understood at all.

Material and methods

Plant material and labelling experiments

Three-year-old, 50–70 cm high *Halimium halimifolium* L. plants, a Mediterranean drought semi-deciduous shrub, were grown in 3 L plastic pots, filled with two parts of potting soil and one part of sand. Plants were fertilized weekly with one-quarter diluted, modified Hoagland´s fertilizer solution [27]. For the experiments, *H. halimifolium* plants were transferred from a greenhouse into the walk-in climate chambers, where they were kept at day/night cycles of 12:12 h, 25:25˚C, 60:60% relative humidity and 500 μmol m^{-2} s^{-1} PPFD during light period. Acclimation to these conditions lasted for one week; plants were supplied with tap water according to their demand and were fertilized as given above.

For labelling experiments, branches of *H. halimifolium* were placed into self-constructed enclosures (see below) the evening before the measurements maintaining the natural orientation of the branches by adjusting the enclosure position. Ninety minutes before ^{13}C-labelling, the branches were cut carefully at the petiole without changing the branch position in the enclosure; they were immediately recut under water and the cut end of the petiole was placed in deionized water. Thereafter (after 90 min) deionized water was replaced by a 10 mM pyruvate solution, *i.e.* the solution was fed to the shoot via the transpiration stream. Control branch samples were left in deionized water for the entire duration of the experiment. Pyruvate (Cambridge Isotope Laboratories, Andover, MA, USA) was 99% ^{13}C-labelled at either the C1 or C2 carbon position dissolved in deionized water. Throughout the entire experiment, continuous online measurements of the isotopic composition of BVOCs and CO_2 as well as photosynthetic gas exchange fluxes were conducted. Two branches were alternately investigated to increase the number of replicates in a given period of time. A picture of an attached *H. halimifolium* branch inside the enclosure system can be found as supplementary information (S1 Fig). All branches were in a good phenological condition and were not flowering.

Measurement system

We set up a measurement system, consisting of three main units, (i) a zero air generator, providing the experimental system with ultra-pure hydrocarbon free air, (ii) the enclosure system to capture trace gas emissions of intact plants or cut branches, and (iii) the analytical section for simultaneous real-time detection of BVOC, CO_2 and H_2O fluxes and their ^{13}C isotopes

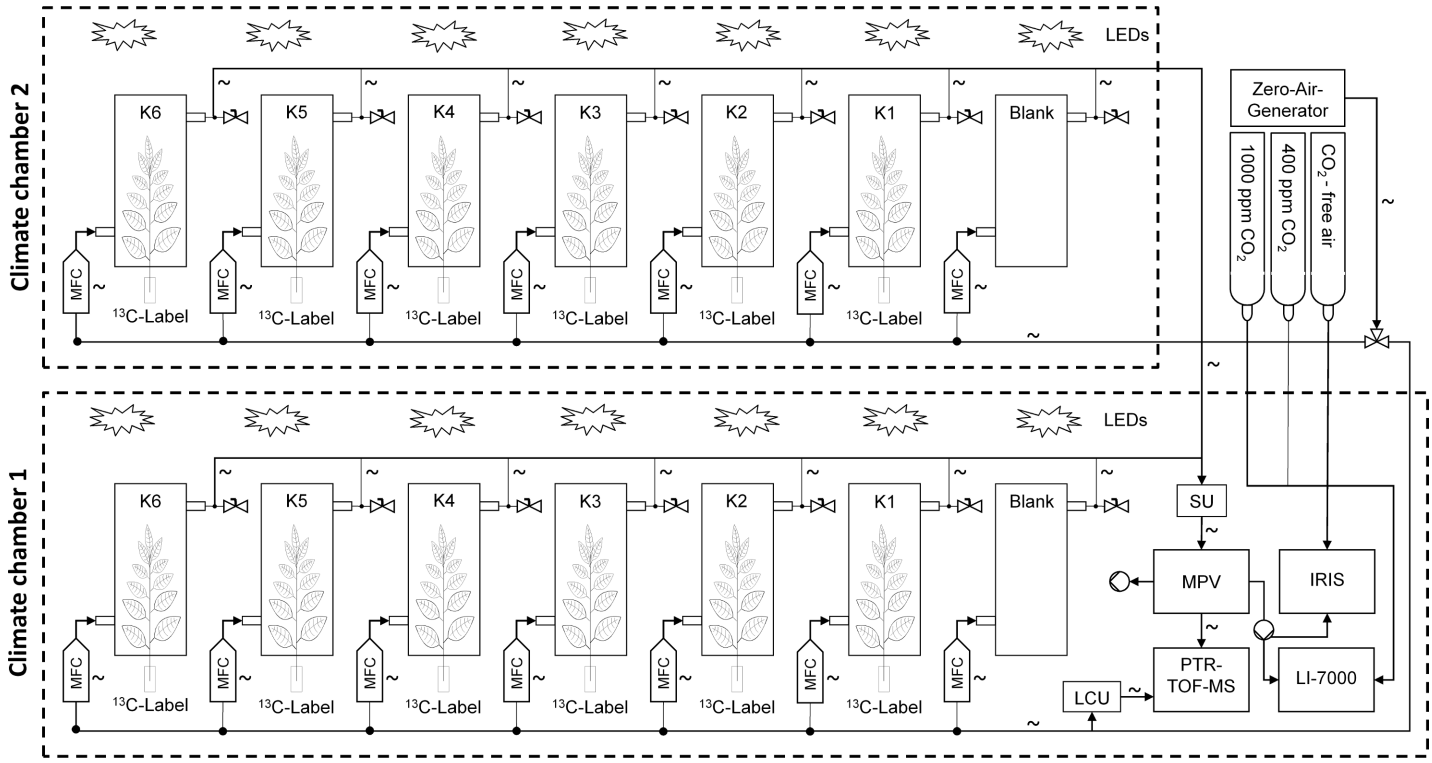

Fig 1. Schematic view of the measurement system. Dotted lines represent the climate chambers. Continuous lines with arrows show the gas tubing and flow direction, while connections are symbolised by a dot. Empty double triangles symbolise valves. Sinuous lines symbolise a heating of the component. "K1-6" stands for enclosures 1–6, "LCU" stands for liquid calibration unit, "MFC" stands for mass flow controller, "MPV" stands for multi-position valve and "SU" stands for switching unit.

https://doi.org/10.1371/journal.pone.0204398.g001

(Fig 1). The analytical section combined, (i) a proton-transfer-reaction time-of-flight mass spectrometer (PTR-TOF-MS, Ionicon Analytic, Innsbruck, Austria), (ii) an isotope ratio infrared spectrometer (IRIS, Thermo Fisher Scientific, Bremen, Germany), and (iii) an infrared gas analyzer (LI-7000 CO_2/H_2O Analyzer; LI-COR, Lincoln, NE, USA). To ensure controlled environmental conditions, the plant enclosures and measuring devices were placed within two walk-in climate chambers (ThermoTec, Weilburg, Germany), entirely light, temperature and humidity controlled. Standardized conditions allowed for monitoring of trace gas emissions in response to changes of single environmental parameters such as temperature or light. The climate chambers were illuminated with LED panels with a maximum photon flux density (PFD) of 1600 μmol m^{-2} s^{-1}, which generated high and uniform illumination without overheating the enclosures.

We constructed a custom-made zero air generator for continuous supply of hydrocarbon-free, humidified and CO_2 controlled zero-air at a flow rate of up to 20 l min^{-1}. It combined a gas pump, a cold trap, in-line vessels filled with soda lime and activated charcoal, a custom made humidifier and a gas cylinder containing synthetic air mixed with 5 Vol.% CO_2 (Messer Austria, Gumpoldskirchen, Austria) for CO_2 enrichment. In addition, the system contained a catalyst module (HPZA-30000, Parker Hannifin Corporation, Lancaster, NY USA) filled with platinum catalyst pellets (Infiltec, Speyer am Rhein, Germany), which efficiently removes nearly all remaining hydrocarbons in the air stream.

The enclosure system consisted seven 600 ml borosilicate glass enclosures (Kummer, Freiburg, Germany), six of them were used as plant enclosures and one was kept empty as a reference. Branches were inserted into the bottomless enclosures and tightly closed with PTFE-foil

at the plant stem. The inlet flow was controlled by mass flow controllers (Omega Engineering, Stamford, CT, USA) and kept constant at 600 ml min^{-1} resulting in a calculated residence time in the enclosures of 60 s. The outlet flow was split to channel enclosure air to the different analytical devices. The response-time of air leaving the enclosure and reaching the PTR-TOF-MS and IRIS/IRGA was less than 4 and 10 seconds, respectively. In operation mode, the analytical instruments were supplied with an air flow of ~ 400 ml min^{-1} resulting in a slight overpressure in the enclosures. To assure chemical inertness, all cuvette system parts were made of glass or PFA, and outlet lines were continuously isolated and heated up to 60˚C to prevent BVOCs adsorption at the tube walls or water condensation. Inside the PTR-TOF-MS mainly polyetheretherketon (PEEK) and metal is used.

The enclosure air temperature increased by 2˚C (from 25±0.5˚C to 27±0.5˚C) during light period, which is an inhered property of enclosure systems and was taken into account in data analysis. A moderate light reduction of 15–20% was compensated by adjusting the height of the enclosures.

The zero air generator and enclosure system were tested by supplying the empty enclosure system with 1000 ml min^{-1} of purified air. All parameters remained stable during one hour of measurements (CO_2 400±1 ppm; H_2O 15000±500 ppm; e.g. acetone 0.2±0.1 ppb; $\delta^{13}CO_2$–4 ±0.5 ‰), there were no substantial differences between single enclosures, nor did the enclosure system have any significant influence on the zero air itself. Compared to climate chamber or even bottled hydrocarbon free synthetic air (Messer Industriegase, Bad Soden, Germany), BVOCs were markedly lower after passing the zero air generator, indicating that the instrument efficiently removed BVOCs from ambient air (S2 Fig)

BVOC detection by PTR-TOF-MS and TD-GC-MS

Online BVOC measurements were conducted with a 4000ultra PTR-TOF-MS (Ionicon Analytic, Innsbruck, Austria). This PTR-TOF-MS version has a built-in internal mass calibration standard (diiodobenzene, m/z: 330.848 and fragments on 203.943), as well as an ion funnel at the end of the drift tube, which focuses the ion beam to the detector allowing BVOCs with higher molecular masses to be analysed more efficiently. We used a multi-position valve controlled by the PTR-TOF-MS software for switching between the enclosures. All sample lines connected to the multi-position valve were continuously flushed to avoid dead end influences.

The PTR-TOF-MS was operated at 2.7 mbar drift pressure, 600 V drift voltage, at an E/N of 120 Td, and drift tube heated to 80ºC. Water impurities were kept on average below 4%, m/z 29.99 was kept on average below 0.2% and oxygen impurities were kept below 6% relative to the primary ions. The mass resolution was 2000 ± 500 m/Δm depending on the compound.

PTR-TOF-MS data post-processing consisted of (i) correction for non-extending and extending dead times as well as the correction for Poisson statistics [28] and iterative residual analysis and cumulative peak fitting [29] using the PTR-TOF Data Analyzer software version 4.48; (ii) normalization of the data to primary ions and water; (iii) background subtraction; (iv) application of calibration factors and (v) synchronization of PTR-TOF-MS data with the IRIS and IRGA data.

We measured non-^{13}C-labelled BVOCs and their isotopologues containing one ^{13}C-atom (denoted as ^{13}C-BVOCs in the following), which were detected at m/z +1. The PTR-TOF-MS technique is a mass-selective technique, thus isomers could be interfering in the measured masses. Therefore, where possible, thermodesorption—gas chromatography mass-spectrometry (TD-GC-MS) was used to verify the results of PTR-TOF-MS. Polar compounds and those with molecular mass <80 amu were not analysed by TD-GC-MS and we assigned these masses to specific compounds according to literature. These compounds were either previously

reported to be emitted by vegetation and/or based on mass accuracy of previously reported PTR-TOF-MS measurements. An overview of possible compounds can be found as supporting information (S1 Table). Moreover, specific compounds such as methyl acetate or kaurene emissions by our *H. halimifolium* plants were validated in previous studies by TD-GC-MS measurements and calibration standards [22,30].

Calibration of the assigned BVOCs was done either with a multicomponent calibration gas standard (1000 ppb ± 5%, Ionicon Analytic, Innsbruck, Austria), liquid standards or via transmission calculations. For selected compounds (gas and liquid water based calibrations) humidity dependent calibrations were done. Liquid calibrations with water-based solutions were done for acetic acid and methyl acetate (Sigma-Aldrich, Taufkirchen, Germany). For sesquiterpenes, trimethylbenzene, 2-hexenal and cis-3-hexenol (Sigma-Aldrich, Taufkirchen, Germany) hexanal-based solutions were used. All calibrations were performed using the Liquid Calibration Unity (LCU, Ionicon Analytic, Innsbruck, Austria). Information on transmission calculations can be found elsewhere [31].

Furthermore, potential losses of some BVOCs in the system were tested by injecting calibration gas via a PFA-tube into the enclosures under normal operation mode (~ 600 ml min^{-1} inlet flow, ~ 400 ml min^{-1} sample flow). For this purpose, we used compound concentrations of 20 ppb, which was within the magnitude of most of the measured compounds. Comparison of calibration gas measurements (normalized counts per second (ncps)) with and without enclosure system influence revealed that losses for toluene, isoprene, α-pinene, acetone, methanol, acetaldehyde and crotonaldehyde were negligible (S3 Fig). Negligible losses can be assured only for these compounds, but given that also low-volatility compounds such as the volatile diterpene (C_{20}) kaurene could be detected (calibrated and cross-validated with GC-MS measurements) [22], makes us confident that strong influences of the measurement system on the considered BVOCs are unlikely. Furthermore, if there were wall losses, the actual emission rates would be even higher than reported.

CO_2 detection by IRIS and IRGA

$^{13}CO_2$ fluxes [nmol min^{-1} m^{-2}] were quantified based on the differences in $^{13}CO_2$ isotopic composition and their concentration between empty and plant-containing enclosures as analyzed by a Delta Ray Isotope Ratio Infrared Spectrometer (IRIS, Thermo Fisher Scientific, Bremen, Germany). IRIS is an optical analyzer for continuous, online measurements of δ^{13}C-CO_2, δ^{18}O-CO_2 and CO_2 mixing ratios in sample gas. The analyzer operates at a sample flow rate of 80 ml min^{-1} with a temporal resolution down to one second and a precision of 0.15 ‰. Net fluxes of $^{13}CO_2$ (e_{13CO2}) were calculated per projected leaf area (s) as:

$$e_{13CO_2} = \frac{u_{in}}{s} * ({}^{13}c_{out} - {}^{13}c_{in})$$

where u_{in} is the molar flow of incoming air calculated as:

$$u_{in} = \frac{V}{t} * \frac{p}{R * T}$$

with V being the gas volume, t being the time, p being the gas pressure, R being ideal gas constant and T being the temperature, and ${}^{13}c_{out}$ /${}^{13}c_{in}$ is the molar fraction of $^{13}CO_2$ at the inlet and outlet of the enclosure calculated as:

$${}^{13}c = \left(\frac{\left(\frac{\delta^{13}CO_2}{1000} + 1\right) * \left(\frac{^{13}C}{^{12}C}\right)_{VPDB}}{\left(\left(\frac{\delta^{13}CO_2}{1000} + 1\right) * \left(\frac{^{13}C}{^{12}C}\right)_{VPDB}\right) + 1} \right) * c_{total}$$

where c_{total} is the mole fraction of total CO_2 in the enclosure and $^{13}C/^{12}C_{VPDB}$ is the isotope ratio of the international standard *Vienna Pee Dee Belemnite*.

The IRIS is equipped with reference gases of different isotopic compositions ($\delta^{13}C_{VPDB}$ of -9.7±0.3‰ /-27.8±0.3‰ and $\delta^{18}O_{VPDB\text{-}CO2}$ of -27.2±0.3‰ /-17.5±0.3‰) (Thermo Fisher Scientific, Bremen, Germany) and CO_2 concentrations (CO_2 mixing ratio of 408 and 1008 ppm) (Messer, Bad Soden, Germany). The isotope reference of CO_2 is automatically diluted with synthetic air carrier gas (Messer, Bad Soden, Germany) to the current CO_2 concentration of the sample gas. Samples were calibrated for isotopic composition throughout the measurements whenever any significant change in the CO_2 mixing ratio in the sample gas occurred, e.g. during the change between plant and blank cuvette. Additionally, automatic calibration for concentration dependency of the analyzer was conducted every night. To cross-validate IRIS measurements, especially temporal dynamics in isotope signature of leaf dark-respired CO_2, we used the in-tube incubation technique as described elsewhere [32].

Photosynthetic gas exchange parameters at branch level were quantified using a differential infrared gas analyzer (LI-7000 CO_2/H_2O Analyzer; LI-COR, Lincoln, NE, USA), which analyzes the CO_2 and H_2O differences between empty and plant containing enclosures. Transpiration rate (E) [mmol m^{-2} s^{-1}], assimilation rate (A) [μmol m^{-2} s^{-1}], and stomatal conductance to water vapor (G_{H2O}) [mmol m^{-2} s^{-1}] were calculated according to Caemmerer and Farquhar [33]. The IRGA was calibrated at least once per week with synthetic air (0 and 408 ppm; (Messer, Bad Soden, Germany)) for CO_2 and just before the experiment for H_2O by a manufacture calibrated GFS3000 (Walz GmbH, Effeltrich, Germany).

Results

Incorporation of ^{13}C label into BVOCs and respiratory CO_2

The PTR-TOF-MS revealed a broad spectrum of over 60 different masses emitted by *H. halimifolium* branches at a considerable amount under controlled conditions (S2 Table); a selection of the most abundant compounds was identified and listed in Table 1 and a characteristic TOF spectrum is shown as supporting information (S4 Fig). Each detected m/z was assigned to specific BVOCs, which were classified as terpenoids (isoprene, monoterpenes, sesquiterpenes), benzenoids (1.3-cyclopentadiene, benzene, toluene, o-xylene, cresol, trimethylbenzene, ethylphenol), oxygenated BVOCs (methanol, acetone, acetic acid, methyl acetate) and green leaf volatiles (hexenal, hexanal, hexenol). Some of the compounds could be cross-validated by GC-MS analysis (Table 1) others were putatively identified on the basis of literature references (S1 Table) or in case of ethylphenol tentatively identified based on mass accuracy.

By far the highest emission rates were detected for methanol (2.1±0.3 nmol m^{-2} s^{-1}), methyl acetate (0.6±0.2 nmol m^{-2} s^{-1}), acetic acid (0.1±0.04 nmol m^{-2} s^{-1}) and monoterpenes (0.1 ±0.002 nmol m^{-2} s^{-1}) (S5 Fig). In general a high variability in BVOC emission rates between plant individuals and between compounds themselves was detected, the former indicated by high standard errors. Especially for acetic acid and methyl acetate highly variable emission rates were found. For methyl acetate, for example, some individuals were high emitters (1.2 ±0.24 nmol m^{-2} s^{-1} for 10 plants out of 17), while others emitted significantly lower amounts (0.008±0.003 nmol m^{-2} s^{-1} for remaining seven plants). However, for other compounds such as monoterpenes and sesquiterpenes, similar emission rates among all plants were found. Interestingly, we also observed significant emission of compounds which are barely reported in literature, like cresol, trimethylbenzene, ethylphenol, toluene or benzene with flux rates of 0.2 ±0.05 pmol m^{-2} s^{-1}, 2.8±0.1 pmol m^{-2} s^{-1}, 0.1±0.03 pmol m^{-2} s^{-1}, 16.5±4.2 pmol m^{-2} s^{-1} and 22.8 ±6.8 pmol m^{-2} s^{-1}, respectively. The mean rates of CO_2 assimilation, transpiration and stomatal

Table 1. Selection of BVOCs emitted by *H. halimifolium*. 5 min-averaged emission rates [pmol m^{-2} s^{-1}] of 15 individual plants in the morning (11 a.m.) under controlled conditions. The m/z, assigned species and their molecular mass are given. Calibration was performed via calibration gas (gaseous), liquid solution (liquid) or via transmission. Some compounds were cross-validated via GC and the match factor given (NIST17 mass spectral library), were nd–not detectable in GC spectra, na–not analyzed. The GC Match for monoterpenes and sesquiterpenes refers to α-pinene and β-caryophyllene. n = 15± standard error (SE). Sensitivities are exemplary shown at a humidity level of 8000 ppm and limits of detection (LODs) are set to 3σ.

m/z	Assigned BVOC	Formula	Molec. mass	Calibration	GC Match	Emission rate	Compound class	Sensitivities	LODs
					[%]	[pmol m^{-2} s^{-1}]		[ncps/ppb]	[ppb]
51.04	Methanol	$CH_4O(H_2O)$	50.06	Gaseous	na	2098 ± 324	Oxyg. BVOC	1.02	1.84
59.05	Acetone	C_3H_6O	58.08	Gaseous	na	9.9 ± 1.2	Oxyg. BVOC	105.5	0.04
61.03	Acetic acid	$C_2H_4O_2$	60.05	Liquid	na	87.4 ± 40	Oxyg. BVOC	35.8	0.12
67.05	Cyclopentadiene	C_5H_6	66.10	Transmission	na	0.04 ± 0.03	Benzenoid	na	na
69.07	Isoprene	C_5H_8	68.12	Gaseous	na	9.0 ± 1.4	Terpenoid	20.9	0.07
75.04	Methyl acetate	$C_3H_6O_2$	74.08	Liquid	na	629.0 ± 209.6	Oxyg. BVOC	44.4	0.05
79.05	Benzene	C_6H_6	78.11	Gaseous	na	22.8 ± 6.8	Benzenoid	85.0	0.02
93.07	Toluene	C_7H_8	92.14	Gaseous	99.4	16.5 ± 4.2	Benzenoid	87.8	0.02
99.08	2-Hexenal	$C_6H_{10}O$	98.14	Liquid	nd	0.1 ± 0.05	GLV	61.7	0.03
101.09	Hexanal/Hexenol	$C_6H_{12}O$	100.16	Liquid	89.7	149.7 ± 68.1	GLV	0.5	2.09
107.08	o-Xylene	C_8H_{10}	106.17	Gaseous	96.1	1.6 ± 0.2	Benzenoid	86.5	0.01
109.1	Cresol	C_7H_8O	108.14	Transmission	nd	0.2 ± 0.05	Benzenoid	na	na
121.1	Trimethylbenzene	C_9H_{12}	120.19	Liquid	91.2	2.8 ± 0.1	Benzenoid	107.6	0.01
123.11	Ethylphenol	$C_8H_{10}O$	122.16	Transmisson	nd	0.1 ± 0.03	Benzenoid	na	na
137.13	Monoterpenes	$C_{10}H_{16}$	136.23	Gaseous	98.2	72.3 ± 2.2	Terpenoid	23.6	0.05
205.19	Sesquiterpenes	$C_{15}H_{24}$	204.35	Liquid	98.3	16.5 ± 0.4	Terpenoid	4.5	0.31

https://doi.org/10.1371/journal.pone.0204398.t001

conductance were 7.4±0.5 μmol m^{-2} s^{-1}, 1.1±0.03 mmol m^{-2} s^{-1} and 113.3±7 mmol m^{-2} s^{-1} respectively.

To shed more light on the biosynthesis pathways of selected BVOC emitted by *H. halimifolium*, position-specific labelling of pyruvate was used. As our measurement system is able to distinguish between ^{12}C and ^{13}C-BVOC fluxes as well as $\delta^{13}CO_2$ emitted, these experiments were set up to test whether BVOC emissions are linked to CO_2 released during daytime.

H. halimifolium branches were fed with either deionised water, [1-13C]- or [2-13C]- position-specific labelled pyruvate solutions (Fig 2, blue, green, and red symbols, respectively), while stomatal conductance (Fig 2A top graph), assimilation rate (Fig 2A bottom graph), $^{13}CO_2$-fluxes (Fig 2B) and $^{13}C/C_{total}$-BVOC ratios (Fig 2C–2J) were continuously analysed. Photosynthetic parameter are shown as a mean of all measured plants (n = 19), whereas $^{13}CO_2$-fluxes and $^{13}C/C_{total}$-BVOC-ratios are separated by treatment. ^{12}C- and ^{13}C-BVOC-fluxes can be found as supplementary information (S6 and S7 Figs).

In response to cutting, a slight decrease of stomatal conductance and assimilation rates occurred (9 and 11%) during the first 2 hours of labelling. Plants, which did not reach stable values, were discharged from the analysis. The response was similar in control plants (deionized water) and labelled branches, suggesting no appreciable influence of the pyruvate solution. While the ^{12}C-BVOC flux of acetic acid (0.14 to 0.15 nmol m^{-2} s^{-1}), methyl acetate (0.34 to 0.32 nmol m^{-2} s^{-1}) and toluene (0.45 to 0.51 nmol m^{-2} s^{-1}) remained constant, the fluxes of cresol (0.002 to 0.006 nmol m^{-2} s^{-1}), trimethylbenzene (0.01 to 0.04 nmol m^{-2} s^{-1}), ethylphenol (0.001 to 0.003 nmol m^{-2} s^{-1}), monoterpenes (0.21 to 0.56 nmol m^{-2} s^{-1}) and sesquiterpenes (0.19 to 0.50 nmol m^{-2} s^{-1}) increased. In unlabelled control plants the $^{13}C/C_{total}$-BVOC ratio did not change significantly over time (Figs 2C–2J and 3). During [1-13C]-PYR labelling slight but significant increase in the heavier BVOC isotopologue (0.5–1%) was recorded (starting a

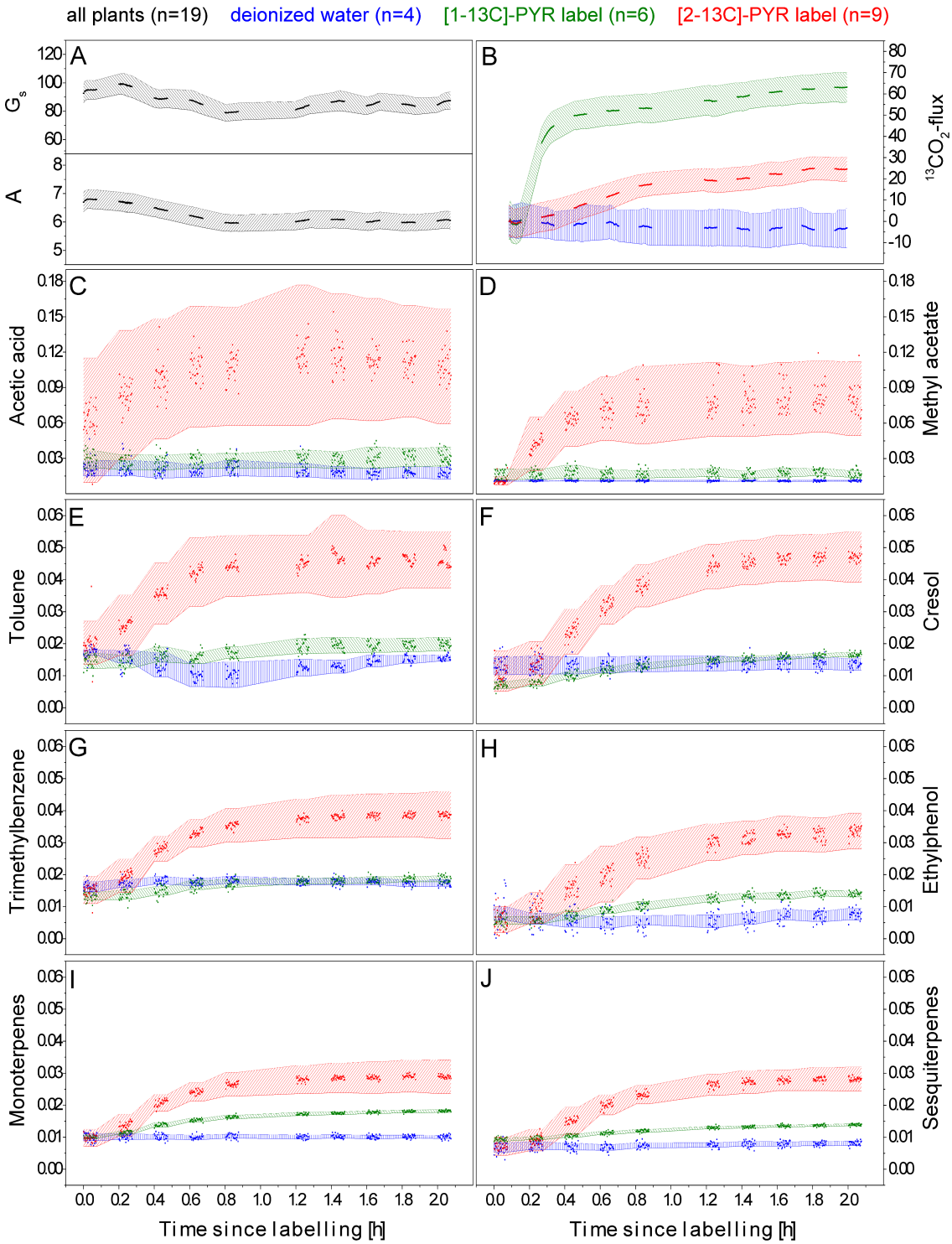

Fig 2. ^{13}C-label incorporation into BVOC- and respiratory CO_2 emissions during position-specific ^{13}C-pyruvate labelling. A: Stomatal conductance (G_s) [mmol m^{-2} s^{-1}] (top graph) and assimilation rate [μmol m^{-2} s^{-1}] (bottom graph). B: $^{13}CO_2$-flux [nmol m^{-2} s^{-1}]. C-J: $^{13}C/C_{total}$-BVOC ratios of acetic acid (C), methyl acetate (D), toluene (E), cresol (F), trimethylbenzene (G), ethylphenol (H), monoterpenes (I), sesquiterpenes (J). Branches were fed with deionised water (blue symbols), a pyruvate solution ^{13}C-labelled at the C1- (green symbols) or the C2 (red symbols) -carbon position. Mean values ± SE (black or coloured shaded area) of n = 19 (black), n = 4 (blue), n = 6 (green) or n = 9 (red) replicates. The labelling started at a time 0 h.

https://doi.org/10.1371/journal.pone.0204398.g002

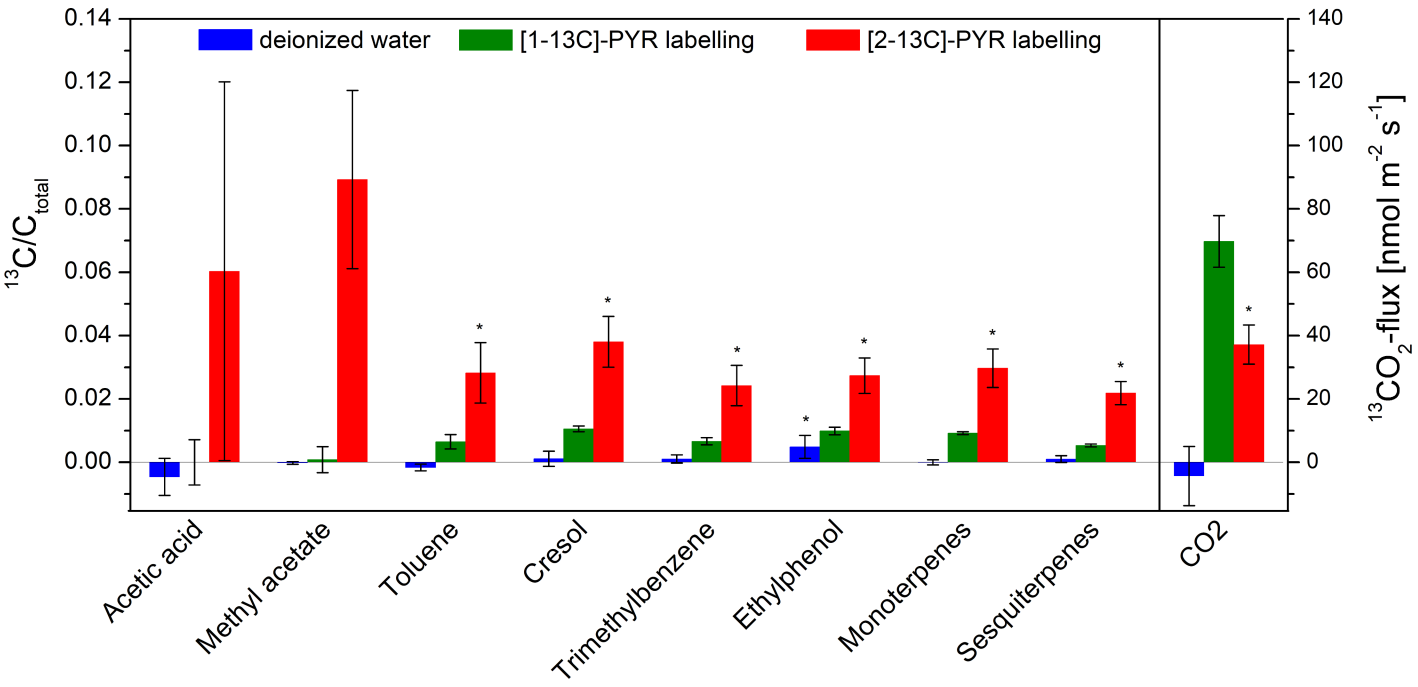

Fig 3. Changes in ^{13}C-label incorporation into BVOCs and CO_2 during 3 h of pyruvate labelling in the light. Branches were fed with deionised water (blue bars), a pyruvate solution ^{13}C-labelled at the C1- (green bars) or the C2 (red bars) -carbon position. ^{13}C-BVOC fluxes of acetic acid, methyl acetate, toluene, cresol, trimethylbenzene, ethylphenol, montoterpenes and sesquiterpenes are shown in relation to their total carbon fluxes (left axis). Label incorporation into CO_2 is shown as change in $^{13}CO_2$-flux [nmol m^{-2} s^{-1}] (right axis). Error bars showing the standard error of n = 4 (blue), n = 6 (green) and n = 9 (orange) replicates. Asterisks indicate significant ($P < 0.05$) differences (t-test).

https://doi.org/10.1371/journal.pone.0204398.g003

few minutes after labelling) in almost all considered compounds, indicating a slight progressive incorporation of ^{13}C (Figs 2C–2J and 3). However, even after 3 h of labelling, the total incorporation of ^{13}C remained minor (<0.1%) in some compounds such as ^{13}C-acetic acid and methyl acetate. Since the labelled C1 position was markedly decarboxylated, a significant increase in $^{13}CO_2$ emissions was detected in our experiments (Figs 2B and 3). In contrast, [2-13C]-PYR labelling caused rapidly increase of the heavier BVOC isotopologues (Figs 2C–2J and 3), while the $^{13}CO_2$ emission during [2-13C]-PYR labelling was threefold lower as compared to [1-13C]-labelling (Fig 2B). Within 3 h of [2-13C]-labelling, significantly increased (2–6%) emission of the heavier BVOC isotopologues were observed for most compounds. As mentioned above, the standard error for acetic acid was high due to large intraspecific variability in the emission rates of individuals for this compound, which, nevertheless, showed an unequivocal incorporation of [2-13C]-PYR label.

Fig 4 shows the temporal dynamics of the label incorporation into BVOCs and CO_2 during [2-13C]-PYR feeding. All considered BVOCs showed an increase in the heavier isotopologue already within the first 10 minutes. All benzenoid/terpenoid compounds (Fig 4 purple and green lines) showed an almost linear incorporation, not reaching a steady state within 50 minutes, whereas the oxygenated compounds (Fig 4 red lines) revealed the strongest incorporation in the first 25 min, reaching almost an equilibrium thereafter. We observed clear differences in the velocity (slope) of ^{13}C-label incorporation into oxygenated compounds and benzenoids/terpenoids, being fastest into methyl acetate and acidic acid, followed by the others. Interestingly, the terpenoid as well as the benzenoid compounds showed patterns comparable to the [2-13C]-label incorporation into emitted CO_2 (Fig 4 black line).

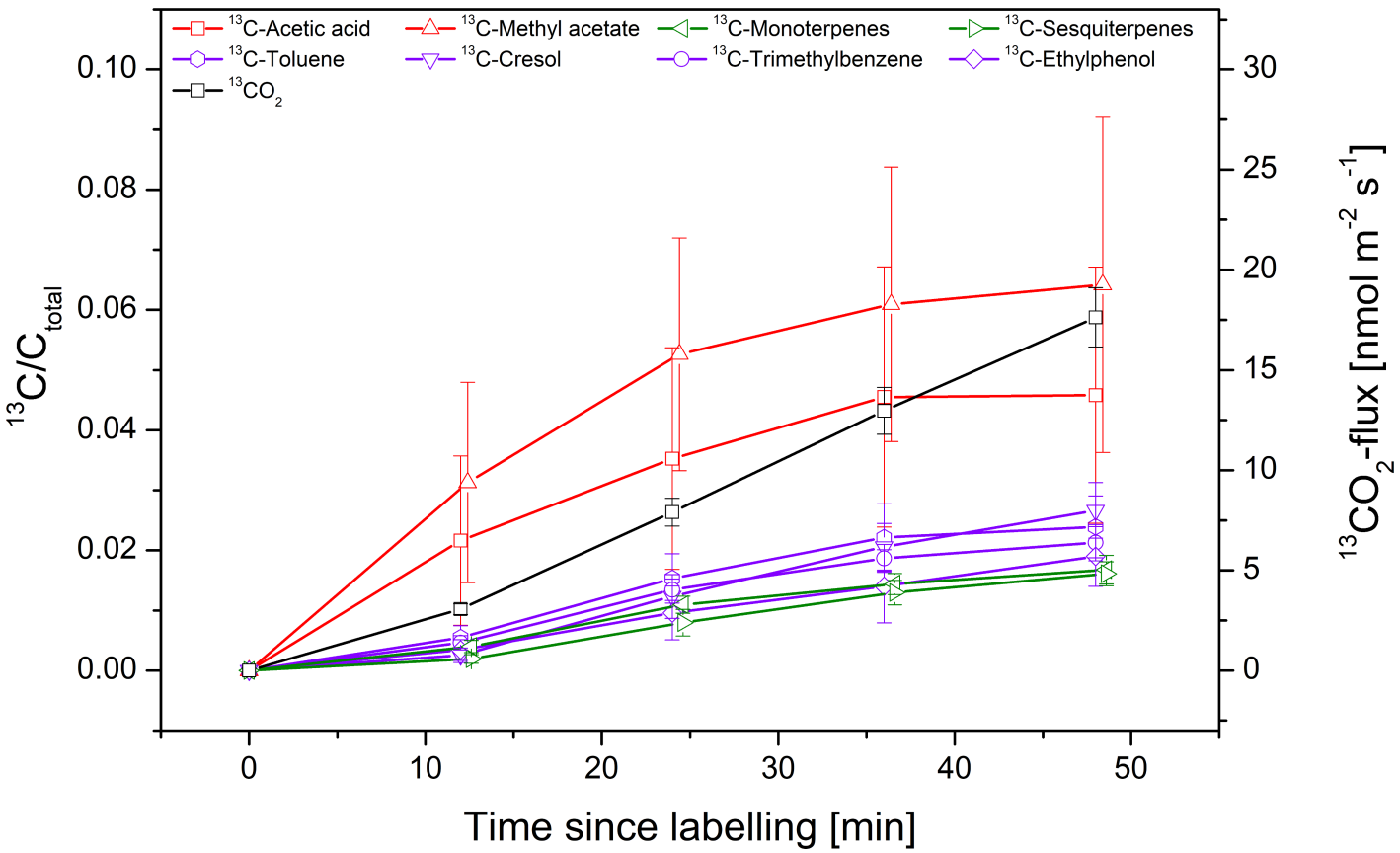

Fig 4. Temporal dynamic of ^{13}C-label incorporation into BVOCs and CO_2 during 50 min of pyruvate labelling in the light. Branches were fed with [2-13C]-position-specific labelled pyruvate. Changes in ^{13}C-BVOC-fluxes of acetic acid (red/square), methyl acetate (red/upward triangle), toluene (purple/hexagon), cresol (purple/downward triangle), trimethylbenzene (purple/circle), ethylphenol (purple/diamond), monoterpenes (green/left triangle) and sesquiterpenes (green/right triangle)) are shown in relation to their total carbon fluxes (left axis). Colour code symbolizes the BVOC class. Label incorporation into CO_2 is shown as change in $^{13}CO_2$-flux [nmol m^{-2} s^{-1}] (black/square/right axis). Error bars show the standard error of n = 9 individual measurements. All samples are taken at the same time steps; the x-axis shift is just for graphical clearness.

https://doi.org/10.1371/journal.pone.0204398.g004

Discussion

In the present study we used position-specific labelling of the key metabolite pyruvate (either [1-13C] or [2-13C]-labelled), which is an efficient tool to trace carbon partitioning at metabolic branching points [15], to elucidate which moiety of the pyruvate molecule is incorporated into volatile compounds or released as $^{13}CO_2$ in the light. The latter can be quantified as measurable $^{13}CO_2$ emission from decarboxylating enzymatic steps mostly of the [1-13C]-atom of pyruvate. If, however, the entire pyruvate molecule is used as a precursor for volatiles, we expect similar ^{13}C-incorporation from both positions. In contrast, if the ^{13}C-tracer is only detected after feeding of [2-13C]-PYR, pyruvate must have been decarboxylated and only the C2-C3-moiety of the molecule is used for production of the volatile compound.

In general, labelling via the transpiration stream in cut branches induces mechanical stress to the plant and should therefore not be applied over many hours. Moreover, additional added metabolites to the plant due to labelling might cause changes in metabolic pathways. Therefore, low concentrated labelling solutions were used to reduce the influences and photosynthetic parameters were continuously controlled and remained relatively stable (Fig 2). On the other hand, a great advantage of position-specific metabolite labelling is, that it enables to trace the fate of specific carbon atoms through plant biochemical cycles, a helpful tool to study

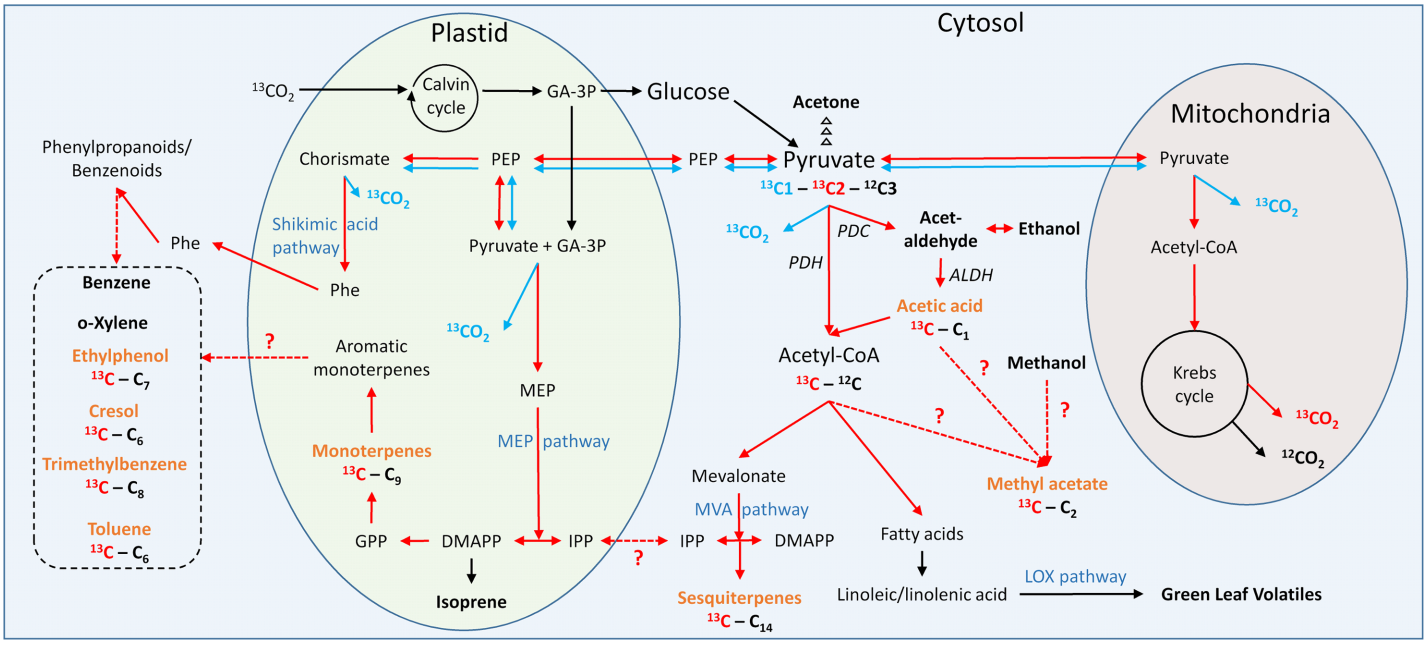

Fig 5. Simplified metabolic scheme of biogenic volatile organic compound (BVOC) biosynthesis in leaves (partly adapted from Dudareva et al. (2006)). Emission rates are given for BVOCs in bold. Bold orange indicates the compounds were we report labelling. Blue arrows symbolize a transfer of the [1-13C]-PYR atom and red arrows symbolize a transfer of the [2-13C]-PYR atom. Dashed arrows symbolize an unclear metabolic pathway. ALDH, aldehyde dehydrogenase; CoA, coenzyme A; DMAPP, dimethylallyl diphosphate; GA-3P, glyceraldehyde-3-phosphate; GPP, geranyl diphosphate; IPP, isopentenyl diphosphate; LOX, lipoxygenase; MEP, 2-C-methyl-D-erythritol 4-phosphate; MVA, mevalonate; PDC, pyruvate decarboxylase; PDH, pyruvate dehydrogenase; PEP, phosphoenolpyruvate; Phe, phenylalanine.

https://doi.org/10.1371/journal.pone.0204398.g005

metabolic branching points. Such position-specific labelling cannot be achieved via fumigation experiments.

The broad range of volatiles and their isotopoloques emitted from the Mediterranean shrub *Halimium halimifolium* indicated a rapid incorporation of ^{13}C to a different extend for each labelled carbon position, which elucidating the production pathways of certain compound groups (Fig 5), as discussed below in detail. Overall, the mass spectra revealed a broad range of organic compounds (> 30) emitted by *H. halimifolium* (S2 Table and S4 Fig), a selection of them could be identified and quantified in this study (Table 1). We chose the compounds with highest emission rates, clearest peak for ^{12}C- and ^{13}C-mass and thorough calibration. The list does not claim completeness but shall give an idea of compounds that are getting labelled via pyruvate during *de novo* biosynthesis. Apart from the well-studied and usually strongly emitted BVOCs like isoprene, monoterpenes, sesquiterpenes, acetaldehyde, formaldehyde and methanol, *H. halimifolium* shoots also released less well studied compounds such as methyl acetate and several benzenoids (benzene, toluene, o-xylene, cresol, trimethylbenzene and ethylphenol).

Biosynthesis of short-chained oxygenated volatiles

We observed a fast incorporation of ^{13}C into short-chain molecules such as acetic acid after feeding the plants with [2-13C]-PYR, which was partially released into the atmosphere due to its high volatility. Such connection of pyruvate with formation and emission of oxygenated compounds has been described in several studies [18,19,34]. The ^{13}C-labelled pyruvate fed to the plant is transported to the leaves via the transpiration stream where it is taken up by leaf cells [19]. In the cytosol, pyruvate can be converted to acetyl-CoA or acetaldehyde as catalyzed by pyruvate dehydrogenase (PDH) and pyruvate decarboxylase (PDC), respectively [3,18].

Both reactions involve decarboxylation of pyruvate accompanied by a release of CO_2. Studies causing enhanced acetaldehyde levels in mesophyll cells demonstrated that this toxic compound is further oxidized by aldehyde dehydrogenase (ALDH) to yield acetate [18]. On the other hand, acetate can also be produced during the exchange of C_2-units between organelles like mitochondria and chloroplasts by acetyl-CoA hydrolysis [35]. Elucidation of the main source of acetate would need further knowledge on the ^{13}C-labelling of acetaldehyde, which, unfortunately, was not provided by our data.

While the biosynthesis of acetic acid via acetaldehyde and acetyl-CoA is well described [3,17,36], much less information is available on the formation of the volatile ester methyl acetate in plants [30]. *H. halimifolium* strongly emitted this compound at rates of 0.6±0.2 nmol m^{-2} s^{-1}, which was an order of magnitude higher than mono- (0.07±0.002 nmol m^{-2} s^{-1}) or sesquiterpenes (0.01±0.0004 nmol m^{-2} s^{-1}) emission and a little higher than reported rates for this species (0.39 ±0.22 nmol m^{-2} s^{-1}) [30]. Noteworthy, methyl acetate (and also acidic acid) emission rates in our study were quite variable between plant individuals in contrast to other emitted compounds (Fig 2). *H. halimifolium* has been characterized as a species with high phenotypic and genotypic plasticity [27,37,38], however, though not being the focus of this study, we were not able to clearly assign high and low emission pattern to individual plants. Since the plants were kept under identical conditions in a controlled climate chamber, we cannot currently disentangle its reasons.

Our labelling patterns suggest that methyl acetate was either derived directly from acetic acid or it was formed from acetyl-CoA, which was produced by conversion of pyruvate and/or activation of acetic acid [30,36,39]. Early work suggested that volatile esters can be synthesised from acetyl-CoA by a transfer of the acetyl moiety to an alcoholic substrate as catalysed by an alcohol acetyltransferase [40]. It has also been proposed that such esters are produced from the lipoxygenase (LOX) pathway, which includes oxidation of cell membrane constituents [41,42]. However, this pathway seems unlikely considering the fast incorporation of the [2-13C]-PYR label in the present study (Fig 4); as we assume that the turnover rates of cell membrane components are much slower. Therefore, the results of our study suggest a link of methyl acetate biosynthesis with the production and emission of acetic acid and confirm earlier assumptions that either acetate or acetyl-CoA are enzymatically methylated [40]. Furthermore, tight linear correlation between ^{12}C- and ^{13}C-fluxes of acetic acid and methyl acetate (R^2 = 0.92 and R^2 = 0.97) support a strong metabolic connection between both compounds (S8 and S9 Figs).

Metabolic link between the biosynthesis of terpenes and volatile aromatics

Besides these short-chained oxygenated compounds, we observed emission and ^{13}C-incorporation into several larger volatile compounds including aromatics and terpenes (Figs 2 and 3). Interestingly, the experiments revealed incorporation of ^{13}C into sesquiterpenes, which has been barely reported before. It is generally assumed that sesquiterpenes are mainly synthesised in the cytosol via the mevalonate pathway (MVA) [43], although there are also some reports about a production in the chloroplasts via the methylerythrol-phosphate (MEP) pathway [44,45]. As expected from the intermediates used in these pathways (MVA: acetyl-CoA, MEP: pyruvate), sesquiterpenes showed a strong incorporation of the C2-C3 moiety of the pyruvate applied. The ^{13}C from [2-13C]-PYR is used in both pathways to form DMAPP and subsequently farnesyl pyrophosphate (FPP), the universal precursor of all sesquiterpenes [46,47], which ultimately results in biosynthesis of ^{13}C-labelled sesquiterpenes [43,48]. In contrast, the weak but distinct incorporation of ^{13}C from [1-13C]-PYR may be explained by photosynthetic re-fixation of emitted $^{13}CO_2$ [17]. The fixed $^{13}CO_2$ contributes to production of glyceraldehyde-3-phosphate, which can be transported to the cytosol, is incorporated into pyruvate derived from glycolysis and subsequently leads to formation of ^{13}C-labelled sesquiterpenes.

Furthermore, crosstalk between MEP- and MVA-pathway via IPP transport into the cytosol can provide an alternative explanation as well [49,50]. Nevertheless, the quick incorporation of the ^{13}C-tracer into sesquiterpenes suggests that these compounds were at least partially produced from *de novo* biosynthesis, which is also supported by our recent study on the same species [22] and is consistent with other work [44,51–53]. However, we detected sesquiterpenes (mainly β-caryophyllene and farnesene) also in storage pools of *H. halimifolium* leaves [22], which indicates that emission is driven by both, a temperature dependent release from stored compounds plus *de novo* production of sesquiterpenes.

Similar to sesquiterpenes, we found strong ^{13}C-labelling of emitted monoterpenes if [2-13C]-PYR was fed to the plants, and a weaker ^{13}C-signal if [1-13C]-PYR was applied. Again, such labelling patterns suggest that the pyruvate taken up by the mesophyll cells was channelled into the plastids and used in the MEP-pathway to form geranyl diphosphate (GPP), the precursor of monoterpenes [43,54]. The MEP pathway starts with the formation of 1-deoxy-d-xylulose 5-phosphate (DXP) by an acyloin condensation of hydroxyl-ethyl-thiamine, derived from the decarboxylated pyruvate, with the C1-aldehyde group of glyceraldehyde 3-phosphate (GA-3P) [49,55]. Thus, due to decarboxylation of pyruvate, the [1-13C]- atom of pyruvate was released as $^{13}CO_2$ and could only be used for terpene biosynthesis after photosynthetic re-fixation. Because of the strong ^{13}C-labelling of monoterpenes, we further conclude that emission is at least partially driven by *de novo* biosynthesis. In good agreement with this assumption, we recently demonstrated that many volatile terpenes (in the order of abundance ρ-cymen-8-ol > α-pinene > eugenol > limonene > terpinene-4-ol > camphene > p-cymene > r-cymene > myrcene) were present in leaf tissue of *H. halimifolium* and many of them seemed to be produced *de novo* in the leaves of this species [22]. Noteworthy, a major portion of the terpenes found in *H. halimifolium* leaves were aromatics such as p-cymen-8-ol, eugenol, p-cymene and m-cymene. Radio-labelling experiments and enzymatic evidence suggest that the aromatic monoterpene p-cymene is produced by an aromatization of γ-terpinene [56]. This compound together with the structurally very similar and biochemically related p-cymene-8-ol and terpinen-4-ol was highly abundant in *H. halimifolium* leaves [22], suggesting a closely linked production.

Besides terpenes, *H. halimifolium* leaves also emitted many aromatic volatiles such as benzene, toluene, trimethylbenzene, o-xylene, cresol and ethylphenol. The emission rates of benzene (22.8±6.8 pmol m^{-2} s^{-1}) and toluene (16.5±4.2 pmol m^{-2} s^{-1}) were in the same range than sesquiterpene emissions. In contrast, release of trimethylbenzene (2.8±0.1 pmol m^{-2} s^{-1}), o-xylene (1.6±0.2 pmol m^{-2} s^{-1}), cresol (0.2±0.05 pmol m^{-2} s^{-1}) and ethylphenol (0.1±0.03 pmol m^{-2} s^{-1}) was considerably lower. The emission rates of toluene observed in the present study were one order of magnitude higher than toluene release of unstressed *Helianthus annuus* leaves (2 pmol m^{-2} s^{-1}), but lower than emissions from stressed sunflower plants (up to 100 pmol m^{-2} s^{-1}) [57]. Consistent with our data, also other studies reported emissions of benzene, toluene, xylene, trimethylbenzene, cresol and phenol from terrestrial vegetation [57–62]. Only ethylphenol emission from plants was not reported before.

The labelling patterns observed for these compounds (Figs 2 and 3) indicate incorporation of ^{13}C from [2-13C]-PYR, whereas, similar to mono- and sesquiterpenes, the [1-13C]-PYR label was not intensively incorporated into volatile benzenoids. The fast incorporation of [2-13C]-PYR label into benzenoids suggest that these compounds are produced *de novo* and emission is not mainly driven from storage pool release. Earlier $^{13}CO_2$ fumigation experiments confirm this assumption at least for toluene [57,58].

Even though benzenoids are assumed to be synthesised in the shikimic acid pathway [47,54], the exact biosynthesis pathway of the selected compounds is still unclear [57,58,60]. Importantly, the shikimic acid pathway starts with the addition of pyruvate to erythrose-

4-phosphate to eventually form shikimate. In subsequent reactions another PEP is added to shikimate-3-phosphate to generate chorismate. This compound, therefore, should contain two ^{13}C-atoms independent if [1-13C]-PYR or [2-13C]-PYR is fed to the plants. Before chorismate is converted to phenylalanine, the assumed precursor for volatile benzenoids, one CO_2 is decarboxylated either by arogenate dehydrogenase or by prephenate dehydratase (PDT), so that phenylalanine would either be double-labelled with ^{13}C if [2-13C]-PYR is fed, or single ^{13}C-labelled if [1-13C]-PYR is fed. The aromatic amino acid phenylalanine is converted to cinnamic acid by the action of phenylalanine ammonia lyase (PAL); volatile benzenoids are then produced by further changes and substitutions on the aromatic ring. Importantly, these modifications involve the release of one ^{13}C from cinnamate most likely leading to benzenoids, which are labelled by one ^{13}C if [2-13C]-PYR was fed and without ^{13}C-label if [1-13C]-PYR was fed. Our results support the idea that volatile benzenoids are formed via the shikimate pathway. On the other hand, they show a very close correlation of benzenoids ^{13}C-labelling with the labelling of terpenes (Fig 4), a high abundance of aromatic terpenes in leaves of *H. halimifolium*, and a very similar chemical structure of these aromatic monoterpenes with the released benzenoids. This highlights the possibility that these compounds might also be derived from the MEP pathway as suggested by Misztal et al. [58]. This hypothesis is supported by the correlation matrix of benzenoids and monoterpenes fluxes (^{12}C-monoterpenes to ^{12}C-toluene ($R^2 = 0.98$), ^{13}C-monoterpenes to ^{13}C-toluene ($R^2 = 0.99$), to ^{13}C-cresol ($R^2 = 0.99$) or to ^{13}C-trimethylbenzene ($R^2 = 0.99$)) (S8 and S9 Figs), indicating a strong connection between these biosynthesis pathways. However, further labelling studies of important intermediates, such as phenylalanine or shikimate, is required to elucidate the pathways responsible.

Day respiratory CO_2 efflux from metabolic branching points

In general, feeding of [1-13C]-labelled pyruvate resulted in substantially increased $^{13}CO_2$-release from the shoots. This increase was threefold stronger as compared to [2-13C]-PYR labelling and detectable immediately after applying the label (Fig 2B), indicating the quantitative relevance of decarboxylation processes during metabolic pathways in plants. As pointed out above, the incorporation of the [1-13C]-atom of pyruvate into the emitted BVOCs was much weaker than the [2-13C]-atom, suggesting that the entire pyruvate molecule is generally not directly used as a precursor of volatile compounds. The remaining weak ^{13}C-label may originate from photosynthetic re-fixation of the decarboxylated gaseous $^{13}CO_2$. Similar CO_2 re-fixation and incorporation into volatiles has been reported in ^{13}C-labelling experiments with other plants [17,19,63]. However, it must be denoted that incorporation of ^{13}C into acetic acid and methyl acetate during [1-13C]-PYR feeding was minor, which is not in line with substantial re-fixation, which would lead to measurable incorporation into these oxygenated compounds. A possible reason for the stronger labelling of e.g. monoterpenes could be the metabolic and spatial proximity to the location of CO_2 fixation in the Calvin cycle. Acetaldehyde, however, a direct precursor of acetic acid, was found to be strongly labelled during $^{13}CO_2$ fumigation of *Prosopis veluntina* [64]. Thus, freshly fixed $^{13}CO_2$ is incorporated into oxygenated volatiles, suggesting [1-13C]-PYR labelling of terpenoids and benzenoids might not just be explained by re-fixation.

Moreover, the strong release of $^{13}CO_2$ after [1-13C]-PYR feeding indicates that decarboxylation of pyruvate is not restricted to dark period. Thus, this non-mitochondrial source of CO_2 seems to contribute considerably to the CO_2 release of leaves during the light period. This observation underlines the importance of CO_2 production during the day, which is still a highly debated topic [12,65]. It is widely accepted that mitochondrial respiration is partly inhibited in the light compared to the dark due to a reorchestration of major pathways,

resulting in a lower CO_2 efflux [10–14]. But it is also assumed that day respiration can account e.g. for at least 5% of the net assimilation in leaves [13]. Though, at the first glance, it might be of minor importance for a total plant carbon balance, nevertheless under unfavourable environmental conditions with low assimilation rates, day respired CO_2 may become an important player in the carbon budget [12]. Nevertheless, since the measurement of day respiratory CO_2 efflux is a nontrivial problem due to strong interaction with photosynthesis and photorespiration, quantifying the amount of day released carbon remains challenging. Hence, precise estimations of day respiratory CO_2 efflux from plants is still scarce [13] and even less is known on its regulation under changing environmental conditions. Here, we can show that one source of non-mitochondrial CO_2 release in the light is the decarboxylation of the C1-atom of pyruvate during biosynthesis of a plethora of plant secondary metabolites such as BVOCs, a carbon source which our approach can help to account for.

Conclusion and perspective

Real-time, synchronised analysis of BVOCs and $\delta^{13}CO_2$ in combination with position-specific labelling of central metabolites provide an enormous potential for biochemical research. Here we demonstrated that position-specific pyruvate labelling combined with on-line BVOC and $^{13}CO_2$ measurement helps to disentangle possible biosynthetic pathways of less studied BVOCs such as methyl acetate or toluene. Methyl acetate might have a biochemical origin strongly connected to acetic acid and methanol and there are hints for a synthesis of some benzenoids via the MEP-pathway. Furthermore, during many of these BVOC biosynthesis pathways the C1-carbon atom of the central metabolite pyruvate is decarboxylated, while the remaining C2-C3-moiety is incorporated. Given the fact, that day respiratory CO_2 efflux is still a big uncertainty in the plant carbon budget, our approach can provide new insights in key determinants controlling the emission of CO_2 in the light period. Despite of increasing awareness of fast reactions in plant emitted trace gases and a tight linkage between primary and secondary carbon metabolism, there is still a lack of understanding the regulation of carbon allocation into these pathways and driving factors, environmental constrains or differences among plant functional groups. Further investigations opens the door for real-time analysis tracing metabolic pathways and carbon turnover under different environmental conditions, which may enhance understanding of regulatory mechanisms in plant carbon metabolism.

Supporting information

S1 Table. Alternative BVOCs for the measured m/z according to literature [58,64,66–78].
(TIF)

S2 Table. Table of detected m/z during labelling experiments. Labelling experiments (L3-L12) for [1-13C]-PYR labelling (C1) or [2-13C]-PYR labelling (C2). Table contains m/z that are clearly distinguishable from background.
(TIF)

S1 Fig. Photograph of a typical *H. halimifolium* branch inside the cuvette system.
(JPG)

S2 Fig. Efficiency of zero-air-generator to purify ambient air. The acetone mixing ratio [ppb] (8 min measurement) in enclosure 1–7 (red to light blue), flushed with 1000 ml min^{-1} of purified air. 25 min measurement of synthetic air (dark blue), supplied from gas vessel (Messer Austria, Gumpoldskirchen, Austria), and 15 min measurement of air in climate chamber (purple). The efficiency is exemplary shown for acetone; most of the other BVOCs revealed similar

pattern.
(TIF)

S3 Fig. BVOC losses due to cuvette system influences. PTR-TOF-MS measurements (ncps background subtracted) of calibration gas (Ionicon Analytic, Innsbruck, Austria) with or without passing the cuvette system.
(TIF)

S4 Fig. Characteristic PTR-TOF-MS spectrum of *H. halimifolium*. Figure shows an averaged (5 min) spectrum of detected BVOCs of one individual plant in the morning (11 a.m.) before a labelling experiment. Spectra shows uncalibrated, background subtracted values in counts per second (cps) plotted by PTR-MS Viewer 3 (Ionicon Analytic, Innsbruck, Austria).
(TIF)

S5 Fig. Proportion of identified BVOCs (Table 1) in respect to their sum.
(TIF)

S6 Fig. ^{12}BVOC-fluxes during position-specific ^{13}C-pyruvate labelling. Fluxes of acetic acid, methyl acetate, toluene, cresol, trimethylbenzene, ethylphenol, monoterpenes and sesquiterpenes are shown in nmol m^{-2} s^{-1}. Symbols show mean values ± SE (black hatched area) of n = 19 replicates. The labelling started at a time 0 h.
(TIF)

S7 Fig. ^{13}C-label incorporation into BVOC and respiratory CO_2 emissions during position-specific ^{13}C-pyruvate labelling. A: $^{13}CO_2$-flux [nmol m^{-2} s^{-1}]. B-I: ^{12}C-BVOC fluxes [nmol m^{-2} s^{-1}] (black lines; left axis) and ^{13}C-BVOC fluxes [nmol m^{-2} s^{-1}] (coloured lines; right axis), of acetic acid (B), methyl acetate (C), toluene (D), cresol (E), trimethylbenzene (F), ethylphenol (G), montoterpenes (H) and sesquiterpenes (I). Branches were fed with deionised water (left panel; A1-I1), a pyruvate solution labelled at the C1- (middle panel; A2-I2) or the C2 (right panel; A3-I3) -carbon position. Symbols show mean values ± SE (black or coloured hatched area) for n = 4 (left), n = 6 (middle) or n = 9 (right) replicates. The labelling started at a time 0 h. The proportion between the light ^{12}C-BVOC isotopologue (left axis) and the corresponding ^{13}C-isotopologue (right axis) is in accordance to the expected proportion of the natural abundance of both isotopologues (Sensu Isotope library, PTR-MS Viewer, Ionicon Analytic, Austria).
(TIF)

S8 Fig. Correlation matrix of ^{12}C-BVOC fluxes during 3 h of labelling.
(TIF)

S9 Fig. Correlation matrix of ^{13}C-BVOC fluxes during 3 h of labelling.
(TIF)

Acknowledgments

The authors gratefully acknowledge the help of Michael Rienks constructing the Zero-Air-Generator and Frederick Wegener for help on technical and experimental aspects.

Author Contributions

Conceptualization: Lukas Fasbender, Christiane Werner.

Data curation: Lukas Fasbender, Ana Maria Yáñez-Serrano.

Formal analysis: Lukas Fasbender, Ana Maria Yáñez-Serrano, David Dubbert.

Investigation: Lukas Fasbender, Ana Maria Yáñez-Serrano, Jürgen Kreuzwieser, Christiane Werner.

Methodology: Lukas Fasbender, Ana Maria Yáñez-Serrano, David Dubbert, Christiane Werner.

Project administration: Christiane Werner.

Resources: Christiane Werner.

Software: Lukas Fasbender, David Dubbert.

Supervision: Christiane Werner.

Validation: Lukas Fasbender, Ana Maria Yáñez-Serrano, Jürgen Kreuzwieser, Christiane Werner.

Visualization: Lukas Fasbender, Ana Maria Yáñez-Serrano.

Writing – original draft: Lukas Fasbender, Ana Maria Yáñez-Serrano, Jürgen Kreuzwieser.

Writing – review & editing: Lukas Fasbender, Ana Maria Yáñez-Serrano, Jürgen Kreuzwieser, Christiane Werner.

References

1. Forster P, Ramaswamy V, Artaxo P, Berntsen T, Betts R, Fahey DW, et al. Changes in atmospheric constituents and in radiative forcing. Chapter 2. Climate Change 2007. The Physical Science Basis; 2007.
2. Sharkey TD, Monson RK. Isoprene research–60 years later, the biology is still enigmatic. Plant, cell & environment. 2017.
3. Karl T, Curtis AJ, Rosenstiel TN, Monson RK, Fall R. Transient releases of acetaldehyde from tree leaves− products of a pyruvate overflow mechanism. Plant, cell & environment. 2002; 25: 1121–1131.
4. Delwiche CF, Sharkey TD. Rapid appearance of 13C in biogenic isoprene when 13CO2 is fed to intact leaves. Plant, cell & environment. 1993; 16: 587–591.
5. Affek HP, Yakir D. Natural abundance carbon isotope composition of isoprene reflects incomplete coupling between isoprene synthesis and photosynthetic carbon flow. Plant Physiology. 2003; 131: 1727–1736. https://doi.org/10.1104/pp.102.012294 PMID: 12692331
6. Kesselmeier J, Staudt M. Biogenic volatile organic compounds (VOC): an overview on emission, physiology and ecology. Journal of atmospheric chemistry. 1999; 33: 23–88.
7. Tcherkez G, Bligny R, Gout E, Mahé A, Hodges M, Cornic G. Respiratory metabolism of illuminated leaves depends on CO2 and O2 conditions. Proceedings of the National Academy of Sciences. 2008; 105: 797–802. https://doi.org/10.1073/pnas.0708947105 PMID: 18184808
8. Werner C, Wegener F, Unger S, Nogues S, Priault P. Short-term dynamics of isotopic composition of leaf-respired CO2 upon darkening. Measurements and implications. Rapid Communications in Mass Spectrometry. 2009; 23: 2428–2438. https://doi.org/10.1002/rcm.4036 PMID: 19603472
9. Sweetlove LJ, Williams TCR, Cheung CY, Ratcliffe RG. Modelling metabolic CO2 evolution–a fresh perspective on respiration. Plant, cell & environment. 2013; 36: 1631–1640.
10. Brooks A, Farquhar GD. Effect of temperature on the CO 2/O 2 specificity of ribulose-1, 5-bisphosphate carboxylase/oxygenase and the rate of respiration in the light. Planta. 1985; 165: 397–406. https://doi.org/10.1007/BF00392238 PMID: 24241146
11. Sweetlove LJ, Beard KFM, Nunes-Nesi A, Fernie AR, Ratcliffe RG. Not just a circle. Flux modes in the plant TCA cycle. Trends in plant science. 2010; 15: 462–470. https://doi.org/10.1016/j.tplants.2010.05.006 PMID: 20554469
12. Tcherkez G, Gauthier P, Buckley TN, Busch FA, Barbour MM, Bruhn D, et al. Leaf day respiration. Low CO2 flux but high significance for metabolism and carbon balance. New Phytologist. 2017; 216: 986–1001. https://doi.org/10.1111/nph.14816 PMID: 28967668
13. Atkin OK, Millar AH, Gardeström P, Day DA. Photosynthesis, carbohydrate metabolism and respiration in leaves of higher plants. Photosynthesis: Springer; 2000. pp. 153–175.

14. Loreto F, Velikova V, Di Marco G. Respiration in the light measured by 12CO 2 emission in 13CO 2 atmosphere in maize leaves. Functional Plant Biology. 2001; 28: 1103–1108.
15. Werner C, Gessler A. Diel variations in the carbon isotope composition of respired CO2 and associated carbon sources: a review of dynamics and mechanisms. Biogeosciences. 2011; 8. https://doi.org/10.5194/bg-8-2437-2011
16. Priault P, Wegener F, Werner C. Pronounced differences in diurnal variation of carbon isotope composition of leaf respired CO2 among functional groups. New Phytologist. 2009; 181: 400–412. https://doi.org/10.1111/j.1469-8137.2008.02665.x PMID: 19121035
17. Kreuzwieser J, Graus M, Wisthaler A, Hansel A, Rennenberg H, Schnitzler J-P. Xylem-transported glucose as an additional carbon source for leaf isoprene formation in Quercus robur. New Phytologist. 2002; 156: 171–178.
18. Graus M, Schnitzler J-P, Hansel A, Cojocariu C, Rennenberg H, Wisthaler A, et al. Transient release of oxygenated volatile organic compounds during light-dark transitions in grey poplar leaves. Plant Physiology. 2004; 135: 1967–1975. https://doi.org/10.1104/pp.104.043240 PMID: 15299129
19. Schnitzler J-P, Graus M, Kreuzwieser J, Heizmann U, Rennenberg H, Wisthaler A, et al. Contribution of different carbon sources to isoprene biosynthesis in poplar leaves. Plant Physiology. 2004; 135: 152–160. https://doi.org/10.1104/pp.103.037374 PMID: 15122010
20. Ghirardo A, Gutknecht J, Zimmer I, Brüggemann N, Schnitzler J-P. Biogenic volatile organic compound and respiratory CO 2 emissions after 13 C-labeling: online tracing of C translocation dynamics in poplar plants. PLoS One. 2011; 6: e17393. https://doi.org/10.1371/journal.pone.0017393 PMID: 21387007
21. Papaefthimiou D, Papanikolaou A, Falara V, Givanoudi S, Kostas S, Kanellis AK. Genus Cistus. A model for exploring labdane-type diterpenes' biosynthesis and a natural source of high value products with biological, aromatic, and pharmacological properties. Frontiers in chemistry. 2014; 2: 35. https://doi.org/10.3389/fchem.2014.00035 PMID: 24967222
22. Yáñez-Serrano Fasbender L, Kreuzwieser J, Dubbert D, Haberstroh S, Lobo-do-Vale R, et al. Volatile diterpene emission by two Mediterranean Cistaceae shrubs. Scientific reports. 2018; 8: 6855. https://doi.org/10.1038/s41598-018-25056-w PMID: 29717178
23. Wegener F, Beyschlag W, Werner C. The magnitude of diurnal variation in carbon isotopic composition of leaf dark respired CO2 correlates with the difference between δ13C of leaf and root material. Functional Plant Biology. 2010; 37: 849–858. https://doi.org/10.1071/FP09224
24. Wegener F, Beyschlag W, Werner C. Dynamic carbon allocation into source and sink tissues determine within-plant differences in carbon isotope ratios. Functional Plant Biology. 2015; 42: 620–629. https://doi.org/10.1071/FP14152
25. Lehmann MM, Wegener F, Werner RA, Werner C. Diel variations in carbon isotopic composition and concentration of organic acids and their impact on plant dark respiration in different species. Plant Biology. 2016; 18: 776–784. https://doi.org/10.1111/plb.12464 PMID: 27086877
26. Lehmann MM, Wegener F, Barthel M, Maurino VG, Siegwolf RTW, Buchmann N, et al. Metabolic Fate of the Carboxyl Groups of Malate and Pyruvate and their Influence on δ13C of Leaf-Respired CO2 during Light Enhanced Dark Respiration. Frontiers in plant science. 2016; 7. https://doi.org/10.3389/fpls.2016.00739 PMID: 27375626
27. Peperkorn R, Werner C, Beyschlag W. Phenotypic plasticity of an invasive acacia versus two native Mediterranean species. Functional Plant Biology. 2005; 32: 933–944. https://doi.org/10.1071/FP04197
28. Titzmann T, Graus M, Müller M, Hansel A, Ostermann A. Improved peak analysis of signals based on counting systems: Illustrated for proton-transfer-reaction time-of-flight mass spectrometry. International Journal of Mass Spectrometry. 2010; 295: 72–77. https://doi.org/10.1016/j.ijms.2010.07.009
29. Müller M, Mikoviny T, Jud W, D'Anna B, Wisthaler A. A new software tool for the analysis of high resolution PTR-TOF mass spectra. Chemometrics and Intelligent Laboratory Systems. 2013; 127: 158–165.
30. Jardine K, Wegener F, Abrell L, van Haren J, Werner C. Phytogenic biosynthesis and emission of methyl acetate. Plant, cell & environment. 2014; 37: 414–424. https://doi.org/10.1111/pce.12164 PMID: 23862653
31. Lindinger W, Hansel A. Analysis of trace gases at ppb levels by proton transfer reaction mass spectrometry (PTR-MS). Plasma Sources Science and Technology. 1997; 6: 111.
32. Werner C, Hasenbein N, Maia R, Beyschlag W, Maguas C. Evaluating high time-resolved changes in carbon isotope ratio of respired CO2 by a rapid in-tube incubation technique. Rapid Communications in Mass Spectrometry. 2007; 21: 1352–1360. https://doi.org/10.1002/rcm.2970 PMID: 17348086
33. Caemmerer S von Farquhar GD. Some relationships between the biochemistry of photosynthesis and the gas exchange of leaves. Planta. 1981; 153: 376–387. https://doi.org/10.1007/BF00384257 PMID: 24276943

34. Jardine KJ, Sommer ED, Saleska SR, Huxman TE, Harley PC, Abrell L. Gas phase measurements of pyruvic acid and its volatile metabolites. Environmental science & technology. 2010; 44: 2454–2460. https://doi.org/10.1021/es903544p PMID: 20210357

35. Liedvogel B, Stumpf PK. Origin of acetate in spinach leaf cell. Plant Physiology. 1982; 69: 897–903. PMID: 16662316

36. MacDonald RC, Kimmerer TW. Metabolism of transpired ethanol by eastern cottonwood (Populus deltoides Bartr.). Plant Physiology. 1993; 102: 173–179. PMID: 12231807

37. Díaz Barradas MC, Zunzunegui M, Garcia Novo E. Autecological traits of Halimium halimifolium in contrasting habitats under a Mediterranean type climate? A review. Folia Geobotanica. 1999; 34: 189–208.

38. Wegener F, Beyschlag W, Werner C. High intraspecific ability to adjust both carbon uptake and allocation under light and nutrient reduction in Halimium halimifolium L. Frontiers in plant science. 2015; 6. https://doi.org/10.3389/fpls.2015.00609 PMID: 26300906

39. Kreuzwieser J, Scheerer U, Rennenberg H. Metabolic origin of acetaldehyde emitted by poplar (Populus tremula× P. alba) trees. Journal of experimental botany. 1999; 50: 757–765.

40. Shalit M, Guterman I, Volpin H, Bar E, Tamari T, Menda N, et al. Volatile ester formation in roses. Identification of an acetyl-coenzyme A. Geraniol/citronellol acetyltransferase in developing rose petals. Plant Physiology. 2003; 131: 1868–1876. https://doi.org/10.1104/pp.102.018572 PMID: 12692346

41. Feussner I, Wasternack C. The lipoxygenase pathway. Annual review of plant biology. 2002; 53: 275–297. https://doi.org/10.1146/annurev.arplant.53.100301.135248 PMID: 12221977

42. Heiden AC, Kobel K, Langebartels C, Schuh-Thomas G, Wildt J. Emissions of oxygenated volatile organic compounds from plants Part I. Emissions from lipoxygenase activity. Journal of atmospheric chemistry. 2003; 45: 143–172.

43. Dudareva N, Negre F, Nagegowda DA, Orlova I. Plant volatiles. Recent advances and future perspectives. Critical reviews in plant sciences. 2006; 25: 417–440.

44. Sallaud C, Rontein D, Onillon S, Jabès F, Duffé P, Giacalone C, et al. A novel pathway for sesquiterpene biosynthesis from Z, Z-farnesyl pyrophosphate in the wild tomato Solanum habrochaites. The Plant Cell. 2009; 21: 301–317. https://doi.org/10.1105/tpc.107.057885 PMID: 19155349

45. May B, Lange BM, Wüst M. Biosynthesis of sesquiterpenes in grape berry exocarp of Vitis vinifera L. Evidence for a transport of farnesyl diphosphate precursors from plastids to the cytosol. Phytochemistry. 2013; 95: 135–144. https://doi.org/10.1016/j.phytochem.2013.07.021 PMID: 23954075

46. McGarvey DJ, Croteau R. Terpenoid metabolism. The Plant Cell. 1995; 7: 1015. https://doi.org/10.1105/tpc.7.7.1015 PMID: 7640522

47. Dudareva N, Pichersky E. Biochemical and molecular genetic aspects of floral scents. Plant Physiology. 2000; 122: 627–634. PMID: 10712525

48. Lichtenthaler HK. The 1-deoxy-D-xylulose-5-phosphate pathway of isoprenoid biosynthesis in plants. Annual review of plant biology. 1999; 50: 47–65.

49. Arigoni D, Sagner S, Latzel C, Eisenreich W, Bacher A, Zenk MH. Terpenoid biosynthesis from 1-deoxy-D-xylulose in higher plants by intramolecular skeletal rearrangement. Proceedings of the National Academy of Sciences. 1997; 94: 10600–10605.

50. Hemmerlin A, Hoeffler J-F, Meyer O, Tritsch D, Kagan IA, Grosdemange-Billiard C, et al. Crosstalk between the cytosolic mevalonate and the plastidial methylerythritol phosphate pathways in tobacco bright yellow-2 cells. Journal of Biological Chemistry. 2003.

51. Duhl TR, Helmig D, Guenther A. Sesquiterpene emissions from vegetation. A review. Biogeosciences Discussions. 2007; 4: 3987–4023.

52. Schuh G, Heiden AC, Hoffmann T, Kahl J, Rockel P, Rudolph J, et al. Emissions of volatile organic compounds from sunflower and beech. Dependence on temperature and light intensity. Journal of atmospheric chemistry. 1997; 27: 291–318.

53. Hansen U, Seufert G. Temperature and light dependence of β-caryophyllene emission rates. Journal of Geophysical Research: Atmospheres. 2003; 108.

54. Dudareva N, Klempien A, Muhlemann JK, Kaplan I. Biosynthesis, function and metabolic engineering of plant volatile organic compounds. New Phytologist. 2013; 198: 16–32. https://doi.org/10.1111/nph.12145 PMID: 23383981

55. Rohmer M, Seemann M, Horbach S, Bringer-Meyer S, Sahm H. Glyceraldehyde 3-phosphate and pyruvate as precursors of isoprenic units in an alternative non-mevalonate pathway for terpenoid biosynthesis. Journal of the American Chemical Society. 1996; 118: 2564–2566.

56. Poulose AJ, Croteau R. Biosynthesis of aromatic monoterpenes. Conversion of γ-terpinene to p-cymene and thymol in Thymus vulgaris L. Archives of Biochemistry and Biophysics. 1978; 187: 307–314. PMID: 666313

57. Heiden AC, Kobel K, Komenda M, Koppmann R, Shao M, Wildt J. Toluene emissions from plants. Geophysical Research Letters. 1999; 26: 1283–1286.

58. Misztal PK, Hewitt CN, Wildt J, Blande JD, Eller ASD, Fares S, et al. Atmospheric benzenoid emissions from plants rival those from fossil fuels. Scientific reports. 2015; 5: 12064. https://doi.org/10.1038/srep12064 PMID: 26165168

59. Penuelas J, Llusia J. Seasonal patterns of non-terpenoid C6–C10 VOC emission from seven Mediterranean woody species. Chemosphere. 2001; 45: 237–244. PMID: 11592412

60. Owen SM, Harley P, Guenther A, Hewitt CN. Light dependency of VOC emissions from selected Mediterranean plant species. Atmospheric Environment. 2002; 36: 3147–3159.

61. Castelyn HD, Appelgryn JJ, Mafa MS, Pretorius ZA, Visser B. Volatiles emitted by leaf rust infected wheat induce a defence response in exposed uninfected wheat seedlings. Australasian Plant Pathology. 2015; 44: 245–254.

62. Effmert U, Dinse C, Piechulla B. Influence of green leaf herbivory by Manduca sexta on floral volatile emission by Nicotiana suaveolens. Plant Physiology. 2008; 146: 1996–2007. https://doi.org/10.1104/pp.107.112326 PMID: 18281418

63. Ghirardo A, Koch K, Taipale R, Zimmer I, Schnitzler J-P, Rinne J. Determination of de novo and pool emissions of terpenes from four common boreal/alpine trees by 13CO2 labelling and PTR-MS analysis. Plant, cell & environment. 2010; 33: 781–792. https://doi.org/10.1111/j.1365-3040.2009.02104.x PMID: 20040067

64. Jardine K, Barron-Gafford GA, Norman JP, Abrell L, Monson RK, Meyers KT, et al. Green leaf volatiles and oxygenated metabolite emission bursts from mesquite branches following light–dark transitions. Photosynthesis research. 2012; 113: 321–333. https://doi.org/10.1007/s11120-012-9746-5 PMID: 22711426

65. Wehr R, Munger JW, McManus JB, Nelson DD, Zahniser MS, Davidson EA, et al. Seasonality of temperate forest photosynthesis and daytime respiration. Nature. 2016; 534: 680–697. https://doi.org/10.1038/nature17966 PMID: 27357794

66. Thekedar B, Szymczak W, Höllriegl V, Hoeschen C, Oeh U. Investigations on the variability of breath gas sampling using PTR-MS. Journal of breath research. 2009; 3: 27007.

67. Cappellin L, Karl T, Probst M, Ismailova O, Winkler PM, Soukoulis C, et al. On quantitative determination of volatile organic compound concentrations using proton transfer reaction time-of-flight mass spectrometry. Environmental science & technology. 2012; 46: 2283–2290.

68. Fares S, Weber R, Park J-H, Gentner D, Karlik J, Goldstein AH. Ozone deposition to an orange orchard. Partitioning between stomatal and non-stomatal sinks. Environmental Pollution. 2012; 169: 258–266. https://doi.org/10.1016/j.envpol.2012.01.030 PMID: 22341155

69. Kaser L, Karl T, Schnitzhofer R, Graus M, Herdlinger-Blatt IS, DiGangi JP, et al. Comparison of different real time VOC measurement techniques in a ponderosa pine forest. Atmospheric Chemistry and Physics. 2013; 13: 2893–2906.

70. Vita F, Taiti C, Pompeiano A, Bazihizina N, Lucarotti V, Mancuso S, et al. Volatile organic compounds in truffle (Tuber magnatum Pico). Comparison of samples from different regions of Italy and from different seasons. Scientific reports. 2015; 5: 12629. https://doi.org/10.1038/srep12629 PMID: 26224388

71. Filella I, Peñuelas J, Llusià J. Dynamics of the enhanced emissions of monoterpenes and methyl salicylate, and decreased uptake of formaldehyde, by Quercus ilex leaves after application of jasmonic acid. New Phytologist. 2006; 169: 135–144. https://doi.org/10.1111/j.1469-8137.2005.01570.x PMID: 16390425

72. Hartungen E von, Wisthaler A, Mikoviny T, Jaksch D, Boscaini E, Dunphy PJ, et al. Proton-transfer-reaction mass spectrometry (PTR-MS) of carboxylic acids. Determination of Henry's law constants and axillary odour investigations. International Journal of Mass Spectrometry. 2004; 239: 243–248.

73. Karl TG, Christian TJ, Yokelson RJ, Artaxo P, Hao WM, Guenther A. The Tropical Forest and Fire Emissions Experiment. Method evaluation of volatile organic compound emissions measured by PTR-MS, FTIR, and GC from tropical biomass burning. Atmospheric Chemistry and Physics. 2007; 7: 5883–5897.

74. Mikoviny T, Kaser L, Wisthaler A. Development and characterization of a high-temperature proton-transfer-reaction mass spectrometer (HT-PTR-MS). Atmospheric Measurement Techniques. 2010; 3: 537–544. https://doi.org/10.5194/amt-3-537-2010

75. Graus M, Müller M, Hansel A. High resolution PTR-TOF. Quantification and formula confirmation of VOC in real time. Journal of the American Society for Mass Spectrometry. 2010; 21: 1037–1044. https://doi.org/10.1016/j.jasms.2010.02.006 PMID: 20335047

76. Brilli F, Gioli B, Ciccioli P, Zona D, Loreto F, Janssens IA, et al. Proton Transfer Reaction Time-of-Flight Mass Spectrometric (PTR-TOF-MS) determination of volatile organic compounds (VOCs) emitted from

a biomass fire developed under stable nocturnal conditions. Atmospheric Environment. 2014; 97: 54–67. https://doi.org/10.1016/j.atmosenv.2014.08.007

77. Jordan A, Haidacher S, Hanel G, Hartungen E, Märk L, Seehauser H, et al. A high resolution and high sensitivity proton-transfer-reaction time-of-flight mass spectrometer (PTR-TOF-MS). International Journal of Mass Spectrometry. 2009; 286: 122–128.

78. Romano A, Hanna GB. Identification and quantification of VOCs by proton transfer reaction time of flight mass spectrometry. An experimental workflow for the optimization of specificity, sensitivity, and accuracy. Journal of Mass Spectrometry. 2018; 53: 287–295. https://doi.org/10.1002/jms.4063 PMID: 29336521